Journal of Solid State Chemistry 184 (2011) 1172–1175

Contents lists available at ScienceDirect

Journal of Solid State Chemistry

journal homepage: www.elsevier.com/locate/jssc

Thermoelectric and microstructural properties of $Pb_{0.9-x}Sn_{0.1}Ge_xTe$ compounds prepared by spinodal decomposition

M. Søndergaard [a], M. Christensen [a], S. Johnsen [a], C. Stiewe [b], T. Dasgupta [b], E. Mueller [b], B.B. Iversen [a,*]

[a] Center for Energy Materials, Department of Chemistry and iNANO, Aarhus University, DK-8000 Aarhus C, Denmark
[b] German Aerospace Center (DLR), Linder Hoehe, DE-51147 Cologne, Germany

ARTICLE INFO

Article history:
Received 11 January 2011
Received in revised form
21 February 2011
Accepted 27 February 2011
Available online 5 March 2011

Keywords:
PbTe–SnTe–GeTe system
Thermoelectrics
Nanostructuring
Spinodal decomposition

ABSTRACT

Three samples of $Pb_{0.9-x}Sn_{0.1}Ge_xTe$ with $x=0.25$, 0.35, 0.6 were prepared by heating the mixtures above the melting point of the constituent elements followed by quenching in water. The $x=0.6$ sample is close to the center of the immiscibility region, while the $x=0.25$ and 0.35 samples are in the Pb rich region inside the spinodal miscibility gap. Microstructural investigations using Powder X-ray Diffraction, Scanning Electron Microscopy and Energy Dispersive X-ray Spectroscopy revealed both GeTe-rich and PbTe-rich phases. The samples were uniaxially hot pressed and the thermoelectric properties were characterized in the temperature range 2–400 K using a commercial apparatus and from 300 to 650 K with a custom designed setup. The best sample ($x=0.6$) reached $zT \approx 0.6$ at 650 K, while the $x=0.25$ and 0.35 samples showed thermal instability at elevated temperatures.

1. Introduction

Thermoelectric materials are able to interconvert heat and electricity, but so far low efficiencies have limited thermoelectricity to niche applications. The efficiency scales with the dimensionless figure of merit, zT

$$zT = \frac{S^2}{\kappa\rho}T$$

where S is the Seebeck coefficient, κ the thermal conductivity, T the absolute temperature and ρ the electrical resistivity. Producing materials with low dimensional nanostructures is a way to improve the figure of merit by enhancing the power factor, S^2/ρ, and reducing the thermal conductivity. The reduction of the thermal conductivity should be done without altering the electronic properties [1–10].

Alloys of tellurides such as Bi_2Te_3 and Sb_2Te_3 are among the most used thermoelectric materials for commercial applications. The tellurium compounds PbTe and GeTe are the main constituents in the high-zT materials Lead Antimony Silver Telluride (LAST) and Tellurium Antimony Germanium Silver (TAGS). Calculations point toward the possibility of reducing the thermal conductivity in small grain size PbSnTe and PbGeTe-materials [11]. Furthermore, the phenomenon of spinodal decomposition was reported as an effective means to reduce the thermal conductivity by nanostructuring in the system of PbSnTe–PbS [12]. The system PbTe–SnTe–GeTe is also reported to contain an immiscibility region for spinodal decomposition due to the large size difference of the cations [13]. Previously, this was utilized by Gelbstein and coworkers [14–17] to make nanostructures in improved p-type materials. The effect of aging treatments on the microstructure and thermal diffusivity has been investigated by Gorsse et al. [18] by heating quenched samples of $Pb_{0.36}Ge_{0.64}Te$ in Ar at 500 °C for different time periods. They found a minimum in thermal diffusivity after 1 min of annealing at 500 °C. The previous reports on the PbTe–SnTe–GeTe system are mostly concerned with the Ge-rich part of the system, near the center of the spinodal miscibility gap. In the present work we study samples with three different compositions $Pb_{0.9-x}Sn_{0.1}Ge_xTe$ ($x=0.25$, 0.35, 0.6), where one is close to the center of the immiscibility region ($x=0.6$), while the two others are in the more Pb-rich region inside the spinodal miscibility gap.

2. Experimental

2.1. Sample preparation

The three samples of $Pb_{0.9-x}Sn_{0.10}Ge_xTe$ ($x=0.25$, 0.35, 0.60) were prepared by mixing stoichiometric amounts of high purity elements (5 N) to a total mass of 3 g per sample. The pure elements were placed in carbon coated quartz ampoules, which were evacuated and sealed. The ampoules were heated to 1123 K in 2 h, held there for 1 h, before quenching in cold water. Samples were cut directly from the prepared ingots and investigations were carried out on the

* Corresponding author. Fax: +45 86 19 61 99.
E-mail address: bo@chem.au.dk (B.B. Iversen).

0022-4596/$ - see front matter © 2011 Elsevier Inc. All rights reserved.
doi:10.1016/j.jssc.2011.02.028

microstructure and the low temperature (2–400 K) bulk thermoelectric properties. Prior to the high temperature (300–650 K) thermoelectric characterization the samples were ground and uniaxially hot pressed because the high temperature setup required different sample sizes. The hot-pressing was carried out in a DC current assisted pressure sintering (Dr Fritsch DSP510 SA) at a temperature of 400 °C and pressure of 95 MPa. This processing of the casted ingots altered the physical properties of the samples.

2.2. Structural investigations

Samples for X-ray powder diffraction were taken from the bulk pieces using a file with fine diamond grains. The powder diffraction patterns were collected on a STOE powder diffractometer equipped with an Imaging Plate Position Sensitive Detector and using a Cu $K\alpha_1$ source in transmission geometry. Scanning Electron Microscopy (SEM) images were measured on the polished surfaces of the samples using a Nova 600 Nano SEM from FEI. Energy Dispersive X-ray Spectroscopy (EDX) maps were recorded on the scanned area.

2.3. Physical properties

The transport properties were measured using a Quantum Design Physical Properties Measurement System (PPMS) from 2 to 400 K. Conducting epoxy was used for mounting wires onto the samples. Resistivity, thermal conductivity and Seebeck coefficient were measured using a 4 point probe technique under quasi steady-state conditions employed by the thermal transport option (TTO) for the PPMS [19]. Hall measurements were carried out on a thin slab cut from the $Pb_{0.55}Sn_{0.1}Ge_{0.35}Te$-sample in varying magnetic fields from −9 to 9 T at room temperature. Thermal analysis was done on the $Pb_{0.55}Sn_{0.1}Ge_{0.35}Te$-sample in a simultaneous Thermal Gravimetric Analysis (TGA) and Differential Scanning Calorimetry (DSC) measurement using a NETZSCH STA449 Jupiter. Spatially resolved measurements of the room temperature Seebeck coefficient were done on polished pieces of bulk samples from the cast ingots using a PANCO Potential Seebeck Microprobe (PSM) [20]. An in-house built facility for the combined measurement of Seebeck coefficient (S) and electrical conductivity (σ) was used to determine the temperature dependence (300–650 K) of these properties on the hot-pressed samples. The experimental setup is particularly beneficial for estimation of zT when the properties of the material may be altered due to thermal cycling. The thermal conductivity values in the 300–650 K temperature range were calculated from the product of the measured density, the thermal diffusivity and the specific heat measured on a Netzsch LFA 457 laser flash apparatus.

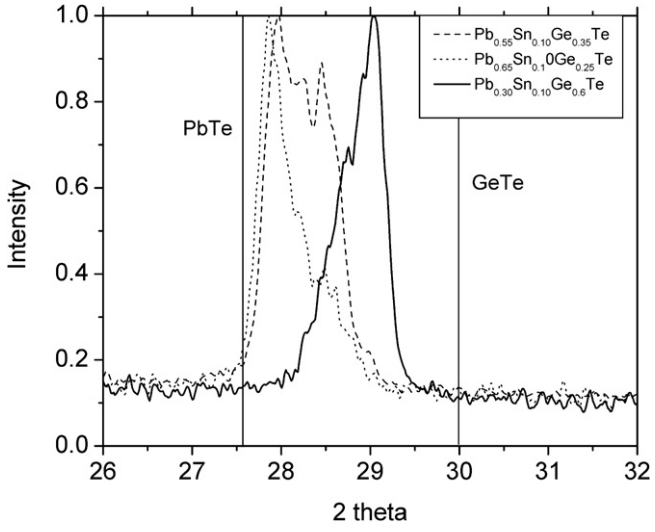

Fig. 1. Powder X-ray Diffraction on the three samples. Dots = $Pb_{0.65}Sn_{0.10}Ge_{0.25}Te$, dashed line = $Pb_{0.55}Sn_{0.10}Ge_{0.35}Te$ and solid line = $Pb_{0.30}Sn_{0.10}Ge_{0.6}Te$. The two straight lines indicate the peak positions of the pure phases of PbTe and GeTe.

3. Results and discussion

3.1. Structural properties

Powder X-ray Diffraction on the three samples revealed broad irregularly shaped peaks as can be seen in Fig. 1. This figure shows an enhancement of the region of interest while complete diffractograms can be found in the supporting information. The peaks of the three samples are positioned between those of pure GeTe and PbTe indicating an extended phase range with various compositions of $Pb_{1-x-y}Ge_xSn_yTe$ and possibly small particle sizes. The SEM-images and EDX-maps of Ge, Pb, Sn and Te confirm the phase separation into regions with Ge-rich and Pb-rich phases, as shown in Fig. 2. The phase domains appear to be on the scale of 1–10 μm. However, the branched structures possibly contain smaller structures on the nanoscale within the microstructures; this is implied by the high resolution SEM image in Fig. 3. Faster quenching rates and/or aging treatments could produce smaller structures, which in turn could lead to improved thermoelectric properties through lower thermal conductivity. Extremely fast cooling was attempted by melt spinning, however the molten compound stuck to the walls of the quartz crucible causing these attempts to fail.

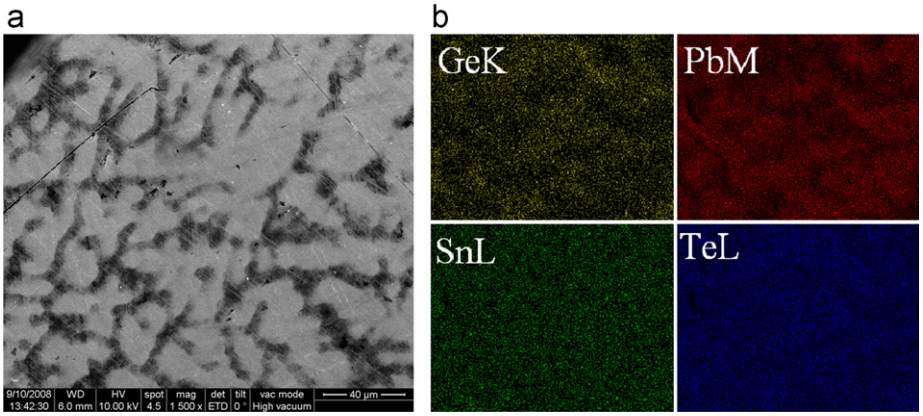

Fig. 2. SEM and EDS images on representative areas of sample $Pb_{0.55}Sn_{0.10}Ge_{0.35}Te$. The $Pb_{0.65}Sn_{0.10}Ge_{0.25}Te$ and $Pb_{0.30}Sn_{0.10}Ge_{0.6}Te$-samples showed similar structures.

Fig. 3. High resolution SEM showing features of a few 100 nm on sample $Pb_{0.55}Sn_{0.10}Ge_{0.35}Te$.

3.2. Physical properties

The electrical resistivity of the samples is shown in Fig. 4. All samples exhibit metallic conductivity as the resistivity increases with temperature. The Ge-rich sample $Pb_{0.3}Sn_{0.1}Ge_{0.6}Te$ has the lowest electrical resistivity. From the Hall measurements on the $Pb_{0.55}Sn_{0.1}Ge_{0.35}Te$ sample at room temperature the charge carrier concentrations were calculated to $4.84 \times 10^{19}\,cm^{-3}$, which corresponds to a heavily doped semiconductor. The Seebeck coefficient of the samples is shown in Fig. 5. For all samples it increases almost linearly with temperature below room temperature, which is consistent with the Mott formula. Due to the thermal excitation of extrinsic charge carriers at higher temperatures a decrease in S (with rising temperatures) is observed for the Pb-rich samples ($x=0.35$ and 0.25) and a corresponding flattening of the resistivity. The Pb-rich samples reveal a change in the resistivity and Seebeck coefficient during the heating and the cooling cycles. TG/DSC-measurement on one of the Pb-rich samples ($x=0.35$) did not show any clear phase transitions up to around 600 °C where Te-evaporation initiates (see supporting information). The Ge-rich sample ($x=0.6$) showed stability up to at least 650 K, where the Seebeck coefficient is still increasing.

The jumps in the resistivities and Seebeck coefficients seen in Figs. 4 and 5 after crushing, hot-pressing and change of measurement setup is a further indication on the change of properties upon heating the samples. This has also been demonstrated by others on similar samples [18]. PXRD on the samples after hot-pressing showed a splitting of the broad peaks into distinct Ge- and Pb-rich phases. Furthermore, there is probably an off-set between the PPMS and the high-temperature setup, and the grinding of the samples introduces larger densities of grain boundaries, which decreases thermal and electrical conductivity.

The average Seebeck coefficients of the samples from Potential Seebeck Microprobe measurements were somewhat lower than the PPMS room temperature data, however, the tendency among samples is the same (see Table 1). Apparently there is a difference between the average Seebeck value measured at different spots and the Seebeck value of the whole sample. The microprobe can potentially give valuable information of the Seebeck coefficient in multiphase systems and the Ge- and Pb-rich phases should be easily distinguished, but since the resolution of the microprobe is maximum 10 µm, the micro- and nanostructures of the samples are too small to have their individual Seebeck coefficients measured.

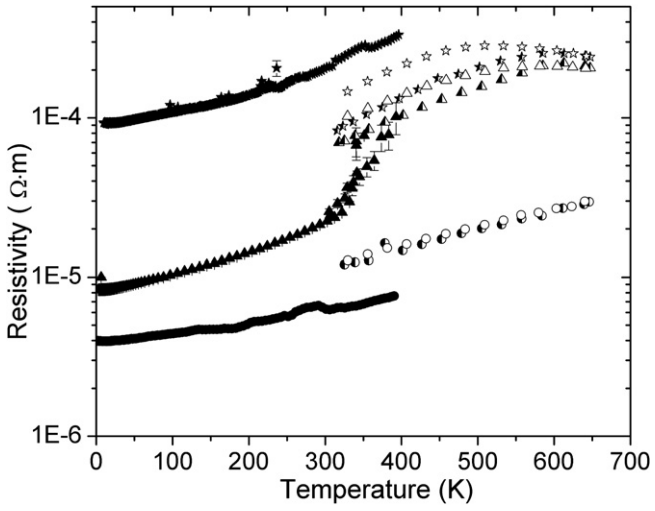

Fig. 4. Resistivity of the compounds $Pb_{0.65}Sn_{0.10}Ge_{0.25}Te$ (stars), $Pb_{0.55}Sn_{0.10}Ge_{0.35}Te$ (triangles) and $Pb_{0.30}Sn_{0.10}Ge_{0.6}Te$ (circles). Filled symbols are data from the PPMS. Half filled and empty symbols are data above room temperature from the heating and cooling cycles, respectively.

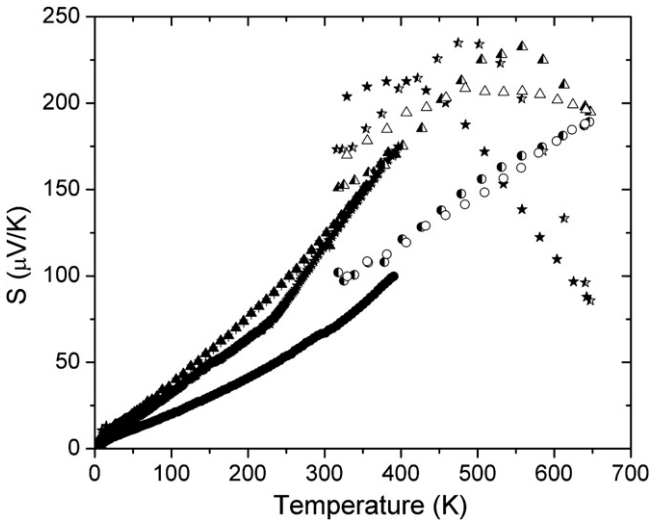

Fig. 5. Seebeck coefficient as function of temperature for the compounds $Pb_{0.65}Sn_{0.10}Ge_{0.25}Te$ (stars), $Pb_{0.55}Sn_{0.10}Ge_{0.35}Te$ (triangles) and $Pb_{0.30}Sn_{0.10}Ge_{0.6}Te$ (circles). Filled symbols are data from the PPMS. Half filled and empty symbols are data above room temperature from the heating and cooling cycles, respectively.

Table 1
Comparison of the Seebeck coefficients measured on a PPMS at 300 K, and average values measured on a Potential Seebeck Microprobe at room temperature.

$Pb_{0.9-x}Sn_{0.1}Ge_xTe$	S (µV/K), $X=0.25$	S (µV/K), $X=0.35$	S (µV/K), $X=0.60$
PSM at 295 K	73 (3)	96 (5)	52 (1)
PPMS at 300 K	117 (1)	125 (1)	67 (1)

Thermal conductivity data is shown in Fig. 6. The Pb-rich samples have a low thermal conductivity around 1 W/(K m) in the temperature range 300–600 K while the $Pb_{0.3}Sn_{0.1}Ge_{0.6}Te$ decreases from 2.2 W/(K m) at 300 K to 1.3 W/(K m) at 670 K.

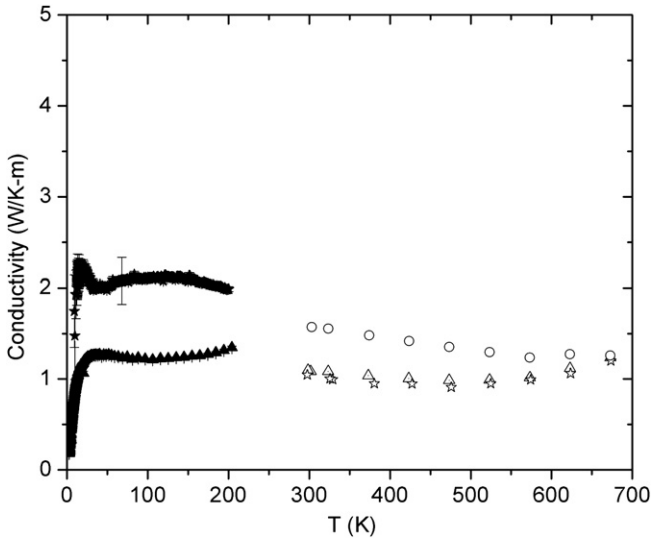

Fig. 6. Thermal conductivity of the compounds $Pb_{0.65}Sn_{0.10}Ge_{0.25}Te$ (stars), $Pb_{0.55}Sn_{0.10}Ge_{0.35}Te$ (triangles) and $Pb_{0.30}Sn_{0.10}Ge_{0.6}Te$ (circles). Filled symbols are data from the PPMS, while empty symbols are from the LFA.

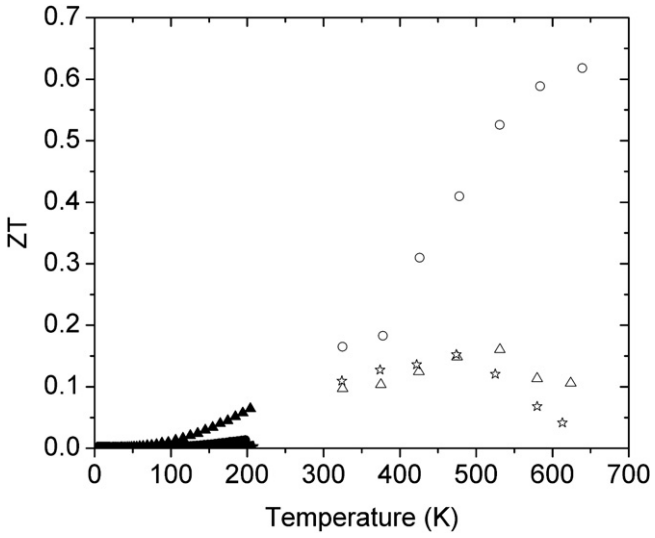

Fig. 7. The figure of merit versus temperature for the three compounds $Pb_{0.65}Sn_{0.10}Ge_{0.25}Te$ (stars), $Pb_{0.55}Sn_{0.10}Ge_{0.35}Te$ (triangles) and $Pb_{0.30}Sn_{0.10}Ge_{0.6}Te$ (circles). Filled symbols are data from the PPMS. Seebeck coefficient and resistivity data are from the heating cycle.

From the S, ρ and κ measurements the zT values are calculated in the range 2–650 K, Fig. 7. Due to their high electrical resistivity the Pb-rich samples only reach zT values around 0.1, while the $Pb_{0.3}Sn_{0.1}Ge_{0.6}Te$ sample reaches $zT=0.6$ at 650 K. Gelbstein et al. [16] also reported $zT=0.6$ at 623 K for this stoichiometry. When comparing the present results with other studies of the PbTe–SnTe–GeTe system, the thermal conductivity above room temperature of $Pb_{0.3}Sn_{0.1}Ge_{0.6}Te$ is in good agreement with values reported in Refs. [13,15] and that of PbTe $\sim$2 W/(K m) at room temperature. The Seebeck coefficient and resistivity of this sample are also in good agreement with values reported in Ref. [13]. Studies by Gelbstein et al. and Gorsse et al. [15–18] have shown that it is possible to produce nanostructures in similar compounds.

4. Conclusion

Spinodal decomposition was utilized to prepare three samples in the PbTe–SnTe–GeTe system with micro- and nanostructures. The two samples in the Pb-rich region of the spinodal miscibility gap showed high electrical resistivity and thermal instability when physical properties were measured at elevated temperatures, while the third sample closest to the center of the spinodal miscibility gap with composition $Pb_{0.3}Sn_{0.1}Ge_{0.6}Te$ was thermally stable and showed a maximum zT of around 0.6 at 650 K.

Acknowledgments

Jacques Chevallier is thanked for help with the Scanning Electron Microscope. This work was supported by the Danish Strategic Research Council (Center for Energy Materials) and the Danish National Research Foundation (Center for Materials Crystallography).

References

[1] L.D. Hicks, M.S. Dresselhaus, Phys. Rev. B 47 (1993) 16631.
[2] M.S. Dresselhaus, G. Chen, M.Y. Tang, R.G. Yang, H. Lee, D.Z. Wang, Z.F. Ren, J.-P. Fleurial, P. Gogna, Adv. Mater. 19 (2007) 1043.
[3] J.R. Sootsman, H. Kong, C. Uher, J.J. D'Angelo, C. Wu, T.P. Hogan, T. Caillat, M.G. Kanatzidis, Angew. Chem. Int. Ed. Engl. 47 (2008) 8618.
[4] R. Venkatasubramanian, E. Siivola, T. Colpitts, B. O'Quinn, Nature 413 (2001) 597.
[5] T. Harman, M. Walsh, B. laforge, G. Turner, J. Electron. Mater. 34 (2005) L19.
[6] M. Christensen, S. Johnsen, B.B. Iversen, Dalton Trans. 39 (2010) 978.
[7] S.K. Bux, J.-P. Fleurial, R.B. Kaner, Chem. Commun. 46 (2010) 8311.
[8] C.J. Vineis, A. Shakouri, A. Majumdar, M.G. Kanatzidis, Adv. Mater. 22 (2010) 3970.
[9] J.R. Sootsman, D.Y. Chung, M.G. Kanatzidis, Angew. Chem. Int. Ed. Engl. 48 (2009) 8616.
[10] B.B. Iversen, J. Mater. Chem. 20 (2010) 10778.
[11] D.M. Rowe, C.M. Bhandari, Appl. Phys. Lett. 47 (1985) 255.
[12] J. Androulakis, et al., J. Am. Chem. Soc. 129 (2007) 9780.
[13] L.V. Yashina, V. Leute, V.I. Shtanov, H.M. Schmidtke, V.S. Neudachina, J. Alloys. Compd. 413 (2006) 133.
[14] Y. Gelbstein, O. Ben-Yehuda, Z. Dashevsky, M.P. Dariel, J. Cryst. Growth 311 (2009) 4289.
[15] Y. Gelbstein, O. Ben-Yehuda, E. Pinhas, T. Edrei, Y. Sadia, Z. Dashevsky, M.P. Dariel, J. Electron. Mater. 38 (2009) 1478.
[16] Y. Gelbstein, B. Dado, O. Ben-Yehuda, Y. Sadia, Z. Dashevsky, M.P. Dariel, Chem. Mater. 22 (2009) 1054.
[17] Y. Gelbstein, Z. Dashevsky, M.P. Dariel, Phys. Status Solidi RRL 1 (2007) 232.
[18] S. Gorsse, P. Bauer Pereira, R. Decourt, E. Sellier, Chem. Mater 22 (2009) 988.
[19] O. Maldonado, Cryogenics 32 (1992) 908.
[20] D. Platzek, G. Karpinski, C. Stiewe, P. Ziolkowski, C. Drasar, E. Muller, in ICT 2005, in: Proceedings of the 24th International Conference on Thermoelectrics, p. 13.